PHOTONICS Research

Folding metamaterials with extremely strong electromagnetic resonance

Harry Miyosi Silalahi,[1] Wei-Fan Chiang,[2] Yi-Hong Shih,[2] Wan-Yi Wei,[1] Jou-Yu Su,[1] and Chia-Yi Huang[1],*

[1]*Department of Applied Physics, Tunghai University, Taichung 40704, China*
[2]*Department of Photonics, Taiwan Cheng Kung University, Tainan 70101, China*
Corresponding author: chiayihuang@thu.edu.tw

Aqueous solutions cannot be detected using transmissive terahertz metamaterials because water strongly absorbs terahertz waves. Transmissive terahertz metamaterials are easier to integrate terahertz emitters and receivers into single and compact devices than reflective terahertz metamaterials. The detection of aqueous solutions using transmissive terahertz metamaterials is a big challenge. This work fabricates a transmissive terahertz metamaterial using a folding metamaterial comprising split-ring resonators (SRRs) with nano-profiles with a high aspect ratio of 41.4. The folding metamaterial has a small transmittance of −49 dB at its resonance frequency, large transmittance contrast of approximately 6×10^4 with respect to the transmittance of its substrate, large refractive index sensitivity of 647 GHz/RIU, and large quality factor of 37. This result arises from the nano-profiles of the SRRs. The nano-profiles increase the surface areas of the SRRs, increasing their surface currents and enhancing the electromagnetic resonance of the folding metamaterial. The folding metamaterial detects a 188-μm-thick rabbit-blood layer that is deposited on it, which cannot be detected by using a common metamaterial. This result reveals that folding metamaterials have potential in detecting the products of live microorganisms with geometrical sizes up to several hundreds of micrometers, such as hydrogen gas, hydrocarbons, and antibodies. © 2022 Chinese Laser Press

https://doi.org/10.1364/PRJ.465746

1. INTRODUCTION

Terahertz waves have attracted much attention due to their unique physical properties, and have been widely used in many fields, such as communications, imaging, and biomedical applications. Terahertz waves have benefits in biomedical applications [1–5]. With large wavelengths and low photon energies, they can be used to detect live human bodies and biomedical samples via their perspective images, so the detection is a nondestructive and non-ionizing method. Terahertz waves can distinguish organic macromolecules because their specific absorptions from molecular rotation, molecular vibration, hydrogen bonding, and van der Waals interaction are mostly in the terahertz region.

Metamaterials comprising split-ring resonators (SRRs) are promising artificial materials because of their abilities to manipulate electromagnetic waves [6–10] and sense dielectric materials [11–14]. Such abilities arise from their electromagnetic resonance. Metamaterials absorb incident electromagnetic waves at their resonance frequencies, reducing their transmittances at the frequencies. Metamaterials with strong electromagnetic resonance are fascinating due to their high contrast ratios, quality factors, and refractive index sensitivities. Such metamaterials have potential in biomedical sensing.

Water can be used to dilute, preserve, and disperse live biomedical samples. Therefore, reflective terahertz metamaterials have been used to sense water-based biomedical samples [15,16]. However, transmissive terahertz metamaterials cannot detect water-based biomedical samples because water strongly absorbs terahertz waves [17]. Transmissive terahertz metamaterials are easier to integrate terahertz emitters and receivers into single and compact devices than reflective terahertz metamaterials. Therefore, the detection of water-based biomedical samples using transmissive terahertz metamaterials is a big challenge.

This work fabricates a transmissive terahertz metamaterial using a folding metamaterial. The folding metamaterial is made by increasing the height of the SRRs of a metamaterial to 20.7 μm and then removing their bulks, leaving SRRs with nano-profiles. The folding metamaterial has an experimental resonance transmittance and quality factor of −49 dB and 37.0, respectively. It has a smaller (larger) resonance transmittance (quality factor) than previous terahertz metamaterials [18–20]. Therefore, the folding metamaterial has extremely strong electromagnetic resonance. The extremely strong electromagnetic resonance arises from the nano-profiles of SRRs. The nano-profiles increase the surface areas of the SRRs, reducing

their resistances and enhancing the electromagnetic resonance of the folding metamaterial. The folding metamaterial has a large transmittance contrast of approximately 6×10^4 with respect to the transmittance of its substrate, and can be used to develop terahertz filters with large transmittance contrasts. Such terahertz filters have potential in photonic integrated circuits, dielectric sensors for the Internet of Things, and super lenses for high-resolution imaging. The folding metamaterial is an excellent dielectric sensor because its refractive index sensitivity (647 GHz/RIU) exceeds those of previous transmissive terahertz metamaterials [11]. The folding metamaterial detects rabbit blood due to its strong electromagnetic resonance as a rabbit-blood layer with a thickness of 188 μm is deposited on it. Therefore, the folding metamaterial comprising SRRs with nano-profiles has great achievement in the detection of aqueous solutions.

2. MATERIALS AND METHODS

Figure 1(a) presents the design of a folding metamaterial, which is made by folding a thin metamaterial. The folding metamaterial comprises SRRs with nano-profiles. A common metamaterial is used to evaluate the electromagnetic resonance
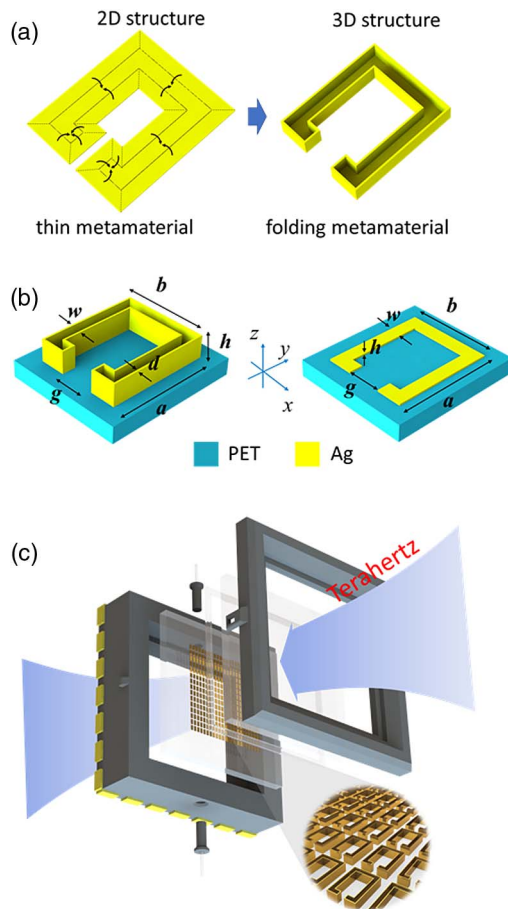
Fig. 1. (a) Design of folding metamaterial. The folding metamaterial comprises SRRs with nano-profiles. (b) Geometrical dimensions of folding and common metamaterials. (c) Illustration of biosensor based on folding metamaterial.
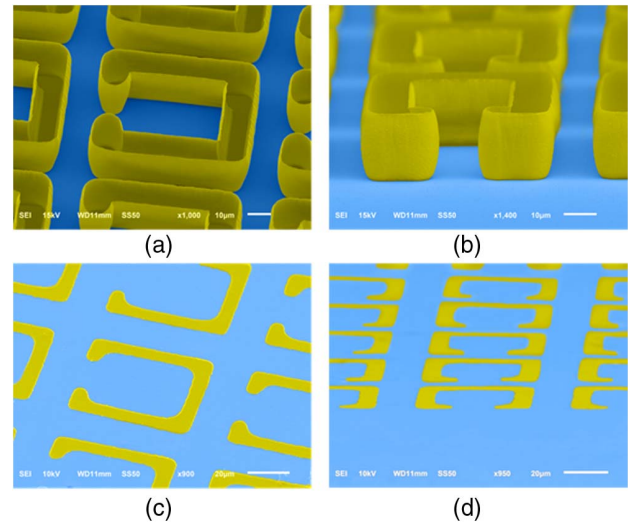
Fig. 2. Scanning electron microscope images of folding metamaterial with height of 20.7 μm at (a) 45° and (b) 80° angles of incidence. Scanning electron microscope images of common metamaterial with height of 500 nm at (c) 45° and (d) 80° angles of incidence.

of the folding metamaterial. The common metamaterial comprises SRRs without nano-profiles. The fabrications of the folding and common metamaterials are presented in Appendix A.

Figure 1(b) presents the geometrical dimensions of folding and common metamaterials. The folding metamaterial is designed to have a width (d), linewidth (w), gap (g), height (h), short side (s), long side (l), period in the x direction, and period in the y direction of 500 nm, 6 μm, 20 μm, 20 μm, 50 μm, 60 μm, 70 μm, and 80 μm, respectively. The folding and common metamaterials have the same geometrical dimensions, but the latter has a height of 500 nm. A folding metamaterial is expected to have extremely strong electromagnetic resonance. The folding metamaterial is a biosensor if it is integrated into a microfluidic channel. Figure 1(c) presents the illustration of a biosensor based on a folding metamaterial.

Figures 2(a) and 2(b) present scanning electron microscope images of the folding metamaterial at 45° and 80° angles of incidence, respectively. The folding metamaterial has a height of 20.7 μm, and the nano-profiles of its SRRs have a width of 500 nm. Therefore, the SRRs in the folding metamaterial have slightly bent nano-profiles due to the high aspect ratio (41.4) of the height (20.7 μm) of the SRRs to the width (500 nm) of their nano-profiles. Figures 2(c) and 2(d) show that the common metamaterial has a height of 500 nm. The folding metamaterial has a larger height than the common metamaterial, so the former has a larger surface area than the latter.

3. RESULTS AND DISCUSSION

A. Experimental Results

Figure 3 presents the experimental and simulated spectra of the folding and common metamaterials. The spectra are obtained from a terahertz spectrometer (TPS 3000, TeraView) in transmission mode, and the polarized direction of incident terahertz waves is set parallel to the gaps of the SRRs of the folding and common metamaterials. The folding (common) metamaterial
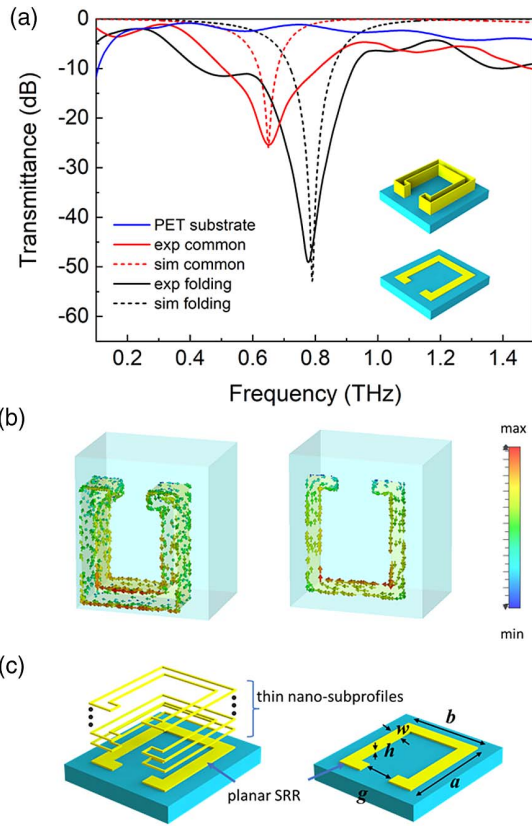
Fig. 3. (a) Experimental (solid lines) and simulated (dashed lines) spectra of folding and common metamaterials. (b) Surface current distributions of SRRs with and without nano-profiles. (c) Theoretical models of SRRs with and without nano-profiles.

has an experimental transmittance of –49 (–25) dB at its resonance frequency of 0.776 (0.654) THz. In addition, the bent wall generates a strong electromagnetic resonance caused by the gap distance being reduced when it is at half its total height. Therefore, the folding metamaterial has extremely strong electromagnetic resonance.

The quality factor of a metamaterial can be used to evaluate the sharpness of its electromagnetic resonance. The quality factor is defined by $f_0/\Delta f_{3\,dB}$, where f_0 is the resonance frequency of the metamaterial, and $\Delta f_{3\,dB}$ is the bandwidth of the cut-off frequencies of the transmittances that exceed the resonance transmittance of the metamaterial by +3 dB [21]. The quality factor is inversely proportional to the resistances of the SRRs of the metamaterial, and so will significantly increase when the resistances are small enough [22].

The folding (common) metamaterial has an experimental quality factor of 37.0 (11.9) due to its $\Delta f_{3\,dB}$ of

0.021 (0.055) THz. The quality factor (37.0) of the folding metamaterial is smaller than that (58.0) of the superconducting metamaterial [23]. However, the superconducting metamaterial cannot be operated at room temperature. In addition, the requirement of a low-temperature facility for the operation of superconducting metamaterials hinders the practical applications of terahertz devices. The folding metamaterial has a larger quality factor than previous terahertz metamaterials operated at room temperature [18–20].

The transmittance contrast C of a metamaterial is given by $C = (T_{sub} - T_{res})/T_{res}$, where T_{res} is the transmittance of a metamaterial at its resonance frequency, and T_{sub} is the transmittance of its substrate at the frequency. The folding metamaterial has a linear (decibel) transmittance of 1.26×10^{-5} (–49 dB) at its resonance frequency, and its polyethylene terephthalate (PET) substrate exhibits a linear (decibel) transmittance of 0.751 (–1.24 dB) at the frequency. Therefore, the folding metamaterial has a transmittance contrast of approximately 6×10^4. The common metamaterial has a linear (decibel) transmittance of 3.16×10^{-3} (–25 dB) at its resonance frequency, and its PET substrate exhibits a linear (decibel) transmittance of 0.65 (–1.84 dB) at the frequency. As a result, the common metamaterial has a transmittance contrast of 2×10^2. The transmittance contrast of the folding metamaterial is higher than that of the common metamaterial by 300 times. This result reveals that the folding metamaterial can be used to develop terahertz filters with large transmittance contrasts. Such terahertz filters have potential in photonic integrated circuits, dielectric sensors for the Internet of Things, and super lenses for high-resolution imaging.

B. Simulated Results

A simulation is performed using CST software to verify the experimental spectra of the folding and common metamaterials. SRRs with and without nano-profiles are used in the simulation, as presented in Fig. 1(b). The PET substrates of the SRRs have a refractive index of 1.73 in the simulation [11]. Silver has an electrical conductivity of 6.30×10^7 S/m in the simulation. A periodical boundary condition is also used in the simulation.

Figure 3(a) presents the simulated spectra of folding and common metamaterials. Table 1 presents a comparison of the simulated and experimental data of folding and common metamaterials. The folding metamaterial has a larger simulated resonance frequency, smaller simulated resonance transmittance, and larger simulated quality factor than the common metamaterial. Simulated data verify the experimental data in Fig. 3(a). Therefore, the folding metamaterial has stronger electromagnetic resonance than the common metamaterial. The folding metamaterial exhibits a discrepancy between the experimental resonance transmittance and the simulated one, and has

Table 1. Comparison of Simulated and Experimental Data of Folding and Common Metamaterials

Type	Resonance Frequency (THz)		Resonance Transmittance (dB)		$\Delta f_{3\,dB}$ (THz)		Quality Factor	
	Sim.	Exp.	Sim.	Exp.	Sim.	Exp.	Sim.	Exp.
Folding	0.790	0.776	–53	–49	0.006	0.021	131.7	37.0
Common	0.650	0.654	–26	–25	0.008	0.055	81.3	11.9

a discrepancy between the experimental quality factor and the simulated one. The discrepancies between the experimental data and simulated data arise from the defects [23] and coupling [21,24,25] of the folding metamaterial.

Figure 3(b) presents the surface current distributions of SRRs with and without nano-profiles. As SRRs with and without nano-profiles have electromagnetic resonance, the excited currents flow on their surfaces. An SRR with a nano-profile has a larger surface current than that without a nano-profile because the former has a larger surface area than the latter. Therefore, the folding metamaterial has stronger electromagnetic resonance than common metamaterials.

C. Theoretical Analysis

An SRR can be regarded as a resistor–inductor–capacitor (RLC) circuit in series [26]. The magnitude $|Z|$ of the impedance of the RLC circuit is given by [27]

$$|Z| = \sqrt{R^2 + \left(\omega L - \frac{1}{\omega C}\right)^2}, \tag{1}$$

where ω is the angular frequency of a normally incident electromagnetic wave; R is the resistance caused by the collision of electrons driven by the electric field of the wave in the SRR; L is the inductance caused by the electric current in the loop of the SRR; and C is the capacitance caused by the opposite charges at the gap of the SRR. As the SRR has electromagnetic resonance, the angular resonance frequency ω_0 of the SRR is given by $\omega_0 = 1/\sqrt{LC}$. Equation (1) reveals that $|Z| = R$ is satisfied at the electromagnetic resonance of the SRR due to $\omega_0 L = 1/\omega_0 C$. Each of the planar SRRs in Fig. 3(c) is an optically thick SRR due to $h \geq 2\delta$, where h and δ are the height and skin depth of that SRR, respectively. The skin depth of a planar SRR at its electromagnetic resonance is given by $\delta = \sqrt{2/\omega_0 \mu_0 \sigma}$, where σ is the conductivity of the SRR, and μ_0 is the permeability in vacuum. R for a planar SRR is given by [26]

$$R = \frac{l}{\sigma A} = \frac{2a + 2b - 4w - g}{\sigma \times w \times \delta}, \tag{2}$$

where l, A, a, b, w, and g are the loop length, surface area, long side, short side, linewidth, and gap of the SRR, respectively. Substituting $\delta = \sqrt{2/\omega_0 \mu_0 \sigma}$ into Eq. (2) yields

$$R = \frac{2a + 2b - 4w - g}{w} \times \sqrt{\frac{\omega_0 \mu_0}{2\sigma}}. \tag{3}$$

Equation (3) reveals that R is a function of the geometrical dimensions and conductivity of the SRR. Suppose a planar SRR is deposited on a substrate with an impedance of Z_{sub}, and air with an impedance of Z_{air} surrounds the SRR. The normalized transmittance T of the SRR at its resonance frequency is given by

$$T = \frac{Z_{sub} + Z_{air}}{Z_{sub}\left(1 + \frac{Z_{air}}{|Z|}\right) + Z_{air}}. \tag{4}$$

Substituting $|Z| = R$ into Eq. (4) yields

$$T = \frac{Z_{sub} + Z_{air}}{Z_{sub}\left(1 + \frac{Z_{air}}{R}\right) + Z_{air}}. \tag{5}$$

Equation (5) depicts that a small resistance in an SRR decreases its resonance transmittance. In addition, Eq. (2) reveals that the resistance of an SRR can be reduced by increasing its surface area. Therefore, an increase in the surface area of an SRR is crucial to enhance its electromagnetic resonance. This work uses the nano-profile structure with a high aspect ratio of 41.4 to increase the surface areas of SRRs, so the folding metamaterial has extremely strong electromagnetic resonance.

Figure 3(c) presents the theoretical models of SRRs with and without nano-profiles. The SRR with the nano-profile comprises a planar SRR and thin nano-subprofiles. The SRR without a nano-profile is a planar SRR. The two planar SRRs in Fig. 3(c) have the same geometrical dimensions. Suppose the planar SRRs have an identical resistance of R, and each of the nano-subprofiles has a resistance of R_{sub}. The resistance R_{nano} of the SRR with the nano-profile is obtained by connecting the planar SRR and nano-subprofiles in parallel, and is given by

$$R_{nano} = \frac{R \times R_{sub}}{R_{sub} + NR}, \tag{6}$$

where N is the number of nano-subprofiles. Equation (6) reveals that $R_{nano} < R$ due to $R_{sub}/(R_{sub} + NR) < 1$. $R_{nano} < R$ depicts that the SRR with the nano-profile has a smaller resistance than that without a nano-profile. In addition, Eq. (5) reveals that an SRR with a small resistance has a small transmittance at its resonance frequency. Therefore, the folding metamaterial has a smaller resonance transmittance than the common metamaterial. This result verifies that the folding metamaterial has stronger electromagnetic resonance than the common metamaterial.

D. Refractive Index Sensitivity

Figure 4(a) displays the near-field distributions of SRRs with and without nano-profiles. An SRR with a nano-profile has a larger hot spot than that without a nano-profile because the former has a larger surface area than the latter. This result reveals that an SRR with a nano-profile has a stronger near field than that without a nano-profile. In other words, an SRR with a nano-profile interacts more with air than that without
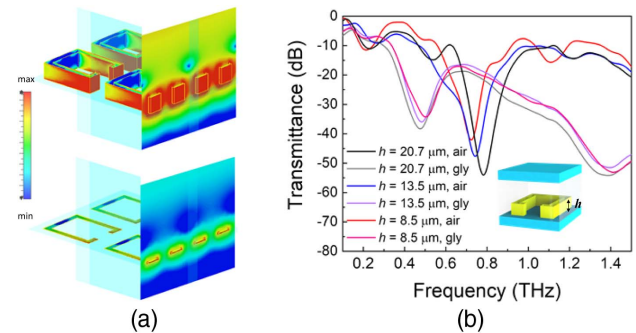
Fig. 4. (a) Near-field distributions of SRRs with and without nano-profiles. (b) Experimental spectra of fluidic cells with folding metamaterials at various heights (h) of SRRs.

a nano-profile. Therefore, the folding metamaterial is highly sensitive to dielectric layers that are deposited on them.

The refractive index sensitivity S of a metamaterial is defined as the ratio of the shifting range of the resonance frequencies of the metamaterial to a change in the refractive indices of the two dielectric materials that are deposited on it separately [28,29]. The effect of the heights of folding metamaterials on their refractive index sensitivities is studied. The folding metamaterials have various heights of 8.5 μm, 13.5 μm, and 20.7 μm in this work. Each of three empty cells is obtained by separating a PET substrate with a folding metamaterial and bare PET substrate using plastic spacers with a thickness of 188 μm. The empty cells are filled with air or glycerol. The fluidic cells with the folding metamaterials are obtained following the filling. Glycerol and air have refractive indices of 1.47 and 1.0, respectively, in the terahertz region [11].

Figure 4(b) presents the experimental spectra of the fluidic cells with the folding metamaterials at various heights (h) of the SRRs. As the air layers in the fluidic cells are replaced with the glycerol layers, the folding metamaterials have frequency shifting ranges of 218 GHz, 260 GHz, and 304 GHz at $h = 8.5$ μm, 13.5 μm, and 20.7 μm, respectively. The folding metamaterials have refractive index sensitivities of 464 (= 218/0.47) GHz/RIU, 553 (= 260/0.47) GHz/RIU, and 647 (= 304/0.47) GHz/RIU at $h = 8.5$ μm, 13.5 μm, and 20.7 μm, respectively. The refractive index sensitivities of the folding metamaterials increase with an increase in their heights. The folding metamaterial at $h = 20.7$ μm has a larger refractive index sensitivity than previous metamaterials due to the large hot spots of the SRRs of the former [30–34]. This result is a great achievement for the development of terahertz metamaterials with large refractive index sensitivities. The unexpected fluctuation of the experimental spectra in Fig. 4(b) arises from the multiple reflections of the fluid cells [35].

A figure of merit (FoM) parameter is interesting to study the sensing performance of the folding metamaterial. The FOM is defined as the ratio of sensitivity (S) and 3 dB-bandwidth ($\Delta f_{3\,dB}$) in this work. The folding metamaterial in this work has an FOM of 30.8 RIU^{-1} (= 0.647/0.021), which is larger than 3.1 RIU^{-1} (= 0.170/0.055) of the common metamaterial. In addition, to compare with previous works of ultrasensitive flexible metamaterial sensors, the sensitivity is defined as the ratio of frequency shift (%) and the change of analyte refractive index (RIU). The sensitivity (%/RIU) of folding metamaterial is 81.9%/RIU (= 38.5%/0.47 RIU) which is larger than those in previous works [36–38].

E. Detection of Rabbit Blood Using Folding Metamaterials

The detection of an aqueous solution using folding and common metamaterials is proposed. The folding and common metamaterials have heights of 20.7 μm and 500 nm, respectively. One of two empty samples is obtained by separating a PET substrate with the folding metamaterial and bare PET substrate using 188-μm-thick plastic spacers, and the other is obtained by separating a PET substrate with the common metamaterial and bare PET substrate using 188-μm-thick plastic spacers. The empty samples are filled with air or rabbit
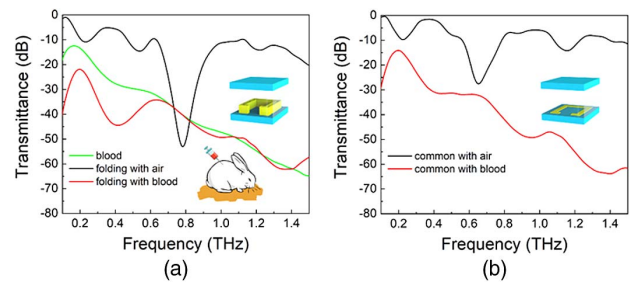
Fig. 5. (a) Experimental spectra of fluidic sample with folding metamaterial imbedded into air and rabbit-blood layers. The green curve is the terahertz spectrum of the rabbit-blood sample without a metamaterial. (b) Experimental spectra of fluidic sample with common metamaterial imbedded into air and rabbit-blood layers.

blood. The fluidic samples with the folding and common metamaterials are obtained following the filling.

A rabbit-blood sample without a metamaterial is used to evaluate the performance of the folding metamaterial. An empty sample is made by separating two bare PET substrates using 188-μm-thick plastic spacers, and then is filled with rabbit blood. Blood samples were taken from a healthy rabbit by a qualified clinician. The blood samples were taken and immediately stored in a blood collection tube with an anticoagulant. The blood samples were centrifuged to split them into blood cells and plasma. The plasma was taken out of the blood collection tube using a syringe. Then, the blood cells were injected into folding and common metamaterial cells. The rabbit-blood sample without a metamaterial is obtained following the filling.

Figure 5(a) presents the experimental spectra of the fluidic sample with the folding metamaterial imbedded into the air and rabbit-blood layers. The green curve in Fig. 5(a) is the terahertz spectrum of the rabbit-blood sample without a metamaterial. The rabbit-blood sample without a metamaterial has low transmittances at the frequencies in its terahertz spectrum. This result reveals that the rabbit-blood layer with a thickness of 188 μm in this sample strongly absorbs the incident terahertz waves.

The black curve in Fig. 5(a) reveals that the fluidic sample with the folding metamaterial imbedded into the air layer has a resonance frequency of 0.788 THz. The resonance frequency arises from the RLC resonance of the folding metamaterial. The transmittance (−40.1 dB) of the rabbit-blood sample without a metamaterial is larger at 0.788 THz than that (−53.0 dB) of the fluidic sample with the folding metamaterial imbedded into the air layer. This result implies that terahertz waves are strong enough to induce the RLC resonance of the folding metamaterial as the air layer in the fluidic sample with the folding metamaterial is replaced by a rabbit-blood layer. The red curve in Fig. 5(a) depicts that the fluidic sample with the folding metamaterial imbedded into the rabbit-blood layer has a significant spectral peak at 0.420 THz. The spectral redshift of the folding metamaterial from 0.788 THz to 0.420 THz arises from the sensitivity of the near fields of its SRRs to a change in the refractive indices of air and rabbit blood. The spectral redshift reveals that the folding metamaterial detects rabbit blood.

Figure 5(b) presents the experimental spectra of the fluidic sample with the common metamaterial imbedded into the air and rabbit-blood layers. The black curve in Fig. 5(b) reveals that the fluidic sample with the common metamaterial imbedded into the air layer has a resonance frequency of 0.655 THz. The transmittance (–33.2 dB) of the rabbit-blood sample without a metamaterial is smaller at 0.655 THz than that (–27.5 dB) of the fluidic sample with the common metamaterial imbedded into the air layer. This result implies that terahertz waves are too weak to induce the RLC resonance of the common metamaterial as the air layer in the fluidic sample with the common metamaterial is replaced by a rabbit-blood layer. The red curve in Fig. 5(b) depicts that the fluidic sample with the common metamaterial imbedded into the rabbit-blood layer has no spectral peak at a frequency smaller than 0.655 THz. No spectral peak reveals that the common metamaterial does not detect rabbit blood.

The results in Figs. 5(a) and 5(b) reveal that the folding metamaterial detects the rabbit-blood layer with a thickness of 188 μm. Therefore, the folding metamaterial has the potential for detecting the products of live microorganisms with geometrical sizes up to several hundreds of micrometers, such as hydrogen gas, hydrocarbons, and antibodies [39–41].

4. CONCLUSION

The new design, fabrication, characterization, simulation, and application of the folding metamaterial comprising SRRs with nano-profiles that have a high aspect ratio of 41.4 are proposed in this work. The resonance transmittance (–49 dB) of the folding metamaterial is smaller than that (–25 dB) of the common metamaterial, and the quality factor (37.0) of the former is larger than that (11.9) of the latter. The SRRs of the folding metamaterial have larger surface currents than those of the common metamaterials because the former has larger surface areas than the latter. Therefore, the folding metamaterial has extremely strong electromagnetic resonance. The folding metamaterial has a large transmittance contrast of approximately 6×10^4 with respect to the transmittance of its substrate, and so has potential in terahertz photonic circuits, dielectric sensors for the Internet of Things, and super lenses for high-resolution imaging.

The folding metamaterial exhibits a large refractive index sensitivity (647 GHz/RIU) of the folding metamaterial, and can be used to develop terahertz metamaterials with large refractive index sensitivities. The folding metamaterial has a significant resonance peak as the rabbit-blood layer with a thickness of 188 μm is deposited on it. Therefore, the folding metamaterial has the potential for sensing the products of live microorganisms with geometrical sizes of up to several hundreds of micrometers, such as hydrogen gas, hydrocarbons, and antibodies.

APPENDIX A: SAMPLE PREPARATION AND FABRICATION

The folding metamaterial is fabricated using a photolithography, thermal evaporation, and lift-off process as presented in Fig. 6(a). A thick positive-photoresist layer (EPG 562, Everlight Chemical Industrial) is deposited on a PET substrate
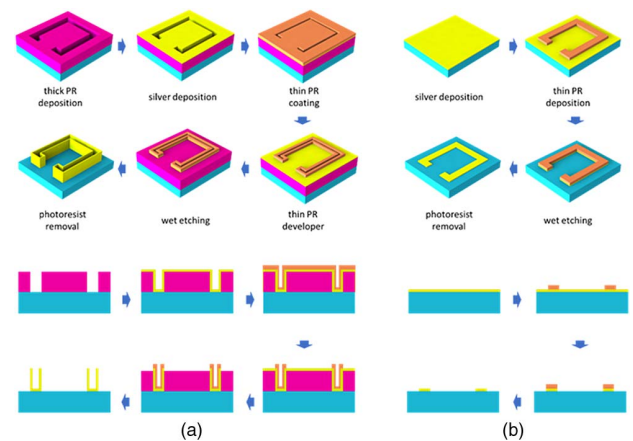

Fig. 6. Fabrication of (a) folding and (b) common metamaterials.

using a spin coater at a spin speed of 1000 r/min for 40 s, and is baked using a hot plate at 110°C for 2 min. The pattern on a photomask is transferred to the positive-photoresist layer at the irradiation of UV light for 60 s. The irradiated positive-photoresist layer is immersed into a developer (EPD 48) for 1 min, and then rinsed in deionized water for 1 min. A positive-photoresist pattern is obtained following the rinse. A silver film with a thickness of 500 nm is deposited on the positive-photoresist pattern using a thermal evaporator. A thin negative-photoresist layer (ENPI202, Everlight Chemical Industrial) is deposited on the silver film using the spin coater at a spin speed of 3000 r/min, and is baked using the hot plate at 100°C for 2 min. The aforementioned pattern on the photomask is transferred to the negative-photoresist layer at the irradiation of UV light for 30 s. The irradiated negative-photoresist layer is developed by a developer, which is prepared by an aqueous solution containing isopropyl alcohol (IPA) with a concentration of 25% (volume fraction), for 50 s, and then is rinsed in deionized water for 1 min. A negative-photoresist pattern is obtained following the rinse. The silver film not covered by the negative-photoresist pattern is etched using a metal etchant for 30 s, then rinsed in deionized water for 1 min. The PET substrate is immersed into acetone to remove the positive and negative photoresists. A folding metamaterial is obtained following the removal of the photoresists.

A common metamaterial is used to evaluate the electromagnetic resonance of the folding metamaterial. Figure 6(b) presents the fabrication process of a common metamaterial. A silver layer with a thickness of 500 nm is deposited on a PET substrate with a thickness of 188 μm using the thermal evaporator. A thin negative-photoresist pattern (ENPI202, Everlight Chemical Industrial) is deposited on the silver layer using the aforementioned photomask via photolithography. The silver film not covered by the negative-photoresist pattern is etched using a metal etchant for 30 s, then rinsed in deionized water for 1 min. The PET substrate is immersed into acetone to remove the negative-photoresist pattern. The common metamaterial is fabricated following the removal of the thin negative-photoresist pattern.

Folding metamaterials at nanoscale may be fabricated via the proposed method in this work. Such metamaterials are able to

manipulate visible light. Folding metamaterials at a nanoscale can be used in biosensing, such as dangerous viruses, body tissues, and cancer cells.

APPENDIX B: TIME-DOMAIN SPECTROSCOPY SYSTEM

All the folding and common metamaterials are measured by using a terahertz spectrometer (TPS 3000, TeraView) in transmission mode, and the polarized direction of incident terahertz waves is set parallel to the gaps of the SRRs of the metamaterials. The infrared light from a femtosecond Ti:sapphire laser (pulse duration: <100 fs; repetition rate: 80 MHz; average power: 300 mW) irradiates a GaAs dipole antenna to generate terahertz waves. The terahertz waves that pass through a metamaterial are received by another GaAs dipole antenna. The time-domain spectrum of the metamaterial is obtained by the antenna, and is converted into its frequency-domain spectrum by fast Fourier transform via a computer. The frequency of the spectrometer ranges from 0.1 THz to 3.0 THz, and its frequency resolution is 3 GHz.

APPENDIX C: SOLID METAMATERIAL

Figure 1(b) shows that the SRRs in the folding metamaterial are hollow because their bulks are removed. It is interesting to study the electromagnetic resonance of a metamaterial with solid SRRs using simulation. The insets in Fig. 7 present the simulated models and surface current distributions of the folding and solid metamaterials. The SRRs in the solid and folding metamaterials [Fig. 1(b)] have the same geometrical dimensions in the simulation, but the SRRs in the former have bulks. Figure 7 displays the simulated spectra of the folding and solid metamaterials with a height of 20.7 μm. The folding metamaterial has stronger electromagnetic resonance than the solid metamaterial since the former has a smaller transmittance at its resonance frequency than the latter. The surface currents are more concentrated at the bottom arms of the SRRs of the folding metamaterial than those of the SRRs of the solid metamaterial. In addition, the currents of the SRRs in the folding metamaterial are distributed over the inner surfaces of their profiles besides the outer surfaces. Therefore, the folding
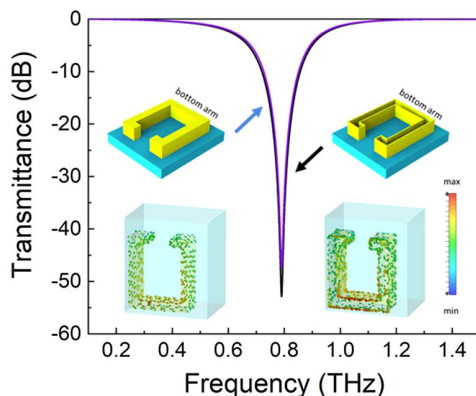
metamaterial has a larger surface current than the solid metamaterial. In other words, the folding metamaterial has stronger electromagnetic resonance than the solid metamaterial.

A previous work reported that a 9-μm-thick solid metamaterial was fabricated using electroplating [42]. The experimental resonance transmittance (−14 dB) of the 9-μm-thick solid metamaterial is larger than that (−49 dB) of the 20.7-μm-thick folding metamaterial, as presented in Fig. 3(a). The 9-μm-thick solid metamaterial exhibits weak electromagnetic resonance because the rough surface caused by the voids and seams of electroplating reduces the current in the metamaterial. Therefore, electroplating cannot fabricate metamaterials with strong electromagnetic resonance. This work proposes a simple method to enhance the electromagnetic resonance of metamaterials by increasing the heights of their SRRs and then removing the bulks of the SRRs, and the method is compatible with all geometrical structures of metamaterials. The folding metamaterial with a nanoscale structure is possible to be fabricated by using electron-beam lithography. However, the electromagnetic resonance frequency of folding metamaterial is blueshifted when its structure is reduced from microscale to the nanoscale.

Disclosures. The authors declare no conflicts of interest.

Data Availability. Data underlying the results presented in this paper may be obtained from the authors upon reasonable request.

REFERENCES

1. J. Zhang, S. Li, and W. Le, "Advances of terahertz technology in neuroscience: current status and a future perspective," iScience **24**, 103548 (2021).
2. L. Sun, L. Zhao, and R.-Y. Peng, "Research progress in the effects of terahertz waves on biomacromolecules," Mil. Med. Res. **8**, 28 (2021).
3. Y. Ma, B. Dong, and C. Lee, "Progress of infrared guided-wave nanophotonic sensors and devices," Nano Converg. **7**, 12 (2020).
4. X. Liu, W. Liu, Z. Ren, Y. Ma, B. Dong, G. Zhou, and C. Lee, "Progress of optomechanical micro/nano sensors: a review," Int. J. Optomechatron. **15**, 120–159 (2021).
5. C. Xu, Z. Ren, J. Wei, and C. Lee, "Reconfigurable terahertz metamaterials: from fundamental principles to advanced 6G applications," iScience **25**, 103799 (2022).
6. W. F. Chiang, H. M. Silalahi, Y. C. Chiang, M. C. Hsu, Y. S. Zhang, J. H. Liu, Y. Yu, C. R. Lee, and C. Y. Huang, "Continuously tunable intensity modulators with large switching contrasts using liquid crystal elastomer films that are deposited with terahertz metamaterials," Opt. Express **28**, 27676–27687 (2020).
7. P. Pitchappa, C. P. Ho, P. Kropelnicki, N. Singh, D.-L. Kwong, and C. Lee, "Dual band complementary metamaterial absorber in near infrared region," J. Appl. Phys. **115**, 193109 (2014).
8. P. Pitchappa, C. Pei Ho, Y. S. Lin, P. Kropelnicki, C. Y. Huang, N. Singh, and C. Lee, "Micro-electro-mechanically tunable metamaterial with enhanced electro-optic performance," Appl. Phys. Lett. **104**, 151104 (2014).
9. P. Pitchappa, A. Kumar, R. Singh, C. Lee, and N. Wang, "Terahertz MEMS metadevices," J. Micromech. Microeng. **31**, 113001 (2021).

Fig. 7. Simulated spectra of the folding and solid metamaterials with a thickness of 20.7 μm. The insets present the simulated models and surface current distributions of folding and solid metamaterials.

10. A. Kumar, A. Solanki, M. Manjappa, S. Ramesh, Y. K. Srivastava, P. Agarwal, T. C. Sum, and R. Singh, "Excitons in 2D perovskites for ultrafast terahertz photonic devices," Sci. Adv. **6**, eaax8821 (2020).

11. H. M. Silalahi, Y. P. Chen, Y. H. Shih, Y. S. Chen, X. Y. Lin, J. H. Liu, and C. Y. Huang, "Floating terahertz metamaterials with extremely large refractive index sensitivities," Photon. Res. **9**, 1970–1978 (2021).

12. W. F. Chiang, S. X. Lin, Y. X. Lee, Y. H. Shih, J. H. Liu, H. M. Silalahi, C. R. Lee, and C. Y. Huang, "Effect of thicknesses of liquid crystal layers on shift of resonance frequencies of metamaterials," Coatings **11**, 578 (2021).

13. K. Shih, P. Pitchappa, L. Jin, C.-H. Chen, R. Singh, and C. Lee, "Nanofluidic terahertz metasensor for sensing in aqueous environment," Appl. Phys. Lett. **113**, 071105 (2018).

14. Y.-S. Lin and Z. Xu, "Reconfigurable metamaterials for optoelectronic applications," Int. J. Optomechatron. **14**, 78–93 (2020).

15. F. Lan, F. Luo, P. Mazumder, Z. Yang, L. Meng, Z. Bao, J. Zhou, Y. Zhang, S. Liang, Z. Shi, A. R. Khan, Z. Zhang, L. Wang, J. Yin, and H. Zeng, "Dual-band refractometric terahertz biosensing with intense wave-matter-overlap microfluidic channel," Biomed. Opt. Express **10**, 3789–3799 (2019).

16. L. Liang, X. Hu, L. Wen, Y. Zhu, X. Yang, J. Zhou, Y. Zhang, I. E. Carranza, J. Grant, C. Jiang, D. R. S. Cumming, B. Li, and Q. Chen, "Unity integration of grating slot waveguide and microfluid for terahertz sensing," Laser Photon. Rev. **12**, 1800078 (2018).

17. K. Shih, P. Pitchappa, M. Manjappa, C. P. Ho, R. Singh, and C. Lee, "Microfluidic metamaterial sensor: selective trapping and remote sensing of microparticles," J. Appl. Phys. **121**, 023102 (2017).

18. N. R. Han, Z. C. Chen, C. S. Lim, B. Ng, and M. H. Hong, "Broadband multi-layer terahertz metamaterials fabrication and characterization on flexible substrates," Opt. Express **19**, 6990–6998 (2011).

19. K. Aydin, I. Bulu, K. Guven, M. Kafesaki, C. M. Soukoulis, and E. Ozbay, "Investigation of magnetic resonances for different split-ring resonator parameters and designs," New J. Phys. **7**, 168 (2005).

20. Z. Wang, Z. Geng, and W. Fang, "Exploring performance of THz metamaterial biosensor based on flexible thin-film," Opt. Express **28**, 26370–26384 (2020).

21. R. Singh, E. Smirnova, A. J. Taylor, J. F. O'Hara, and W. Zhang, "Optically thin terahertz metamaterials," Opt. Express **16**, 6537–6543 (2008).

22. N. Gneiding, O. Zhuromskyy, E. Shamonina, and U. Peschel, "Circuit model optimization of a nano split ring resonator dimer antenna operating in infrared spectral range," J. Appl. Phys. **116**, 164311 (2014).

23. C. H. Zhang, J. B. Wu, B. B. Jin, Z. M. Ji, L. Kang, W. W. Xu, J. Chen, M. Tonouchi, and P. H. Wu, "Low-loss terahertz metamaterial from superconducting niobium nitride films," Opt. Express **20**, 42–47 (2012).

24. J. Wu, B. Jin, Y. Xue, C. Zhang, H. Dai, L. Zhang, C. Cao, L. Kang, W. Xu, J. Chen, and P. Wu, "Tuning of superconducting niobium nitride terahertz metamaterials," Opt. Express **19**, 12021–12026 (2011).

25. R. Singh, A. K. Azad, J. F. O'Hara, A. J. Taylor, and W. Zhang, "Effect of metal permittivity on resonant properties of terahertz metamaterials," Opt. Lett. **33**, 1506–1508 (2008).

26. R. Marqués, F. Mesa, J. Martel, and F. Medina, "Comparative analysis of edge-and broadside-coupled split ring resonators for metamaterial

design-theory and experiments," IEEE Trans. Antennas Propag. **51**, 2572–2581 (2003).

27. D. R. Chowdhury, J. F. O'Hara, A. J. Taylor, and A. K. Azad, "Orthogonally twisted planar concentric split ring resonators towards strong near field coupled terahertz metamaterials," Appl. Phys. Lett. **104**, 101105 (2014).

28. R. Cheng, L. Xu, X. Yu, L. Zou, Y. Shen, and X. Deng, "High-sensitivity biosensor for identification of protein based on terahertz Fano resonance metasurfaces," Opt. Commun. **473**, 125850 (2020).

29. Y. Li, X. Chen, F. Hu, D. Li, H. Teng, Q. Rong, W. Zhang, J. Han, and H. Liang, "Four resonators based high sensitive terahertz metamaterial biosensor used for measuring concentration of protein," J. Phys. D **52**, 095105 (2019).

30. K. Meng, S. J. Park, A. D. Burnett, T. Gill, C. D. Wood, M. Rosamond, L. H. Li, L. Chen, D. R. Bacon, J. R. Freeman, P. Dean, Y. H. Ahn, E. H. Linfield, A. G. Davies, and J. E. Cunningham, "Increasing the sensitivity of terahertz split ring resonator metamaterials for dielectric sensing by localized substrate etching," Opt. Express **27**, 23164–23172 (2019).

31. S. J. Park, J. T. Hong, S. J. Choi, H. S. Kim, W. K. Park, S. T. Han, J. Y. Park, S. Lee, D. S. Kim, and Y. H. Ahn, "Detection of microorganisms using terahertz metamaterials," Sci. Rep. **4**, 4988 (2014).

32. F. Taleb, I. Al-Naib, and M. Koch, "Free-standing complementary asymmetric metasurface for terahertz sensing applications," Sensors **20**, 2265 (2020).

33. S. Wang, L. Xia, H. Mao, X. Jiang, S. Yan, H. Wang, D. Wei, H. Cui, and C. Du, "Terahertz biosensing based on a polarization-insensitive metamaterial," IEEE Photon. Technol. Lett. **28**, 986–989 (2016).

34. X. Yan, M. Yang, Z. Zhang, L. Liang, D. Wei, M. Wang, M. Zhang, T. Wang, L. Liu, J. Xie, and J. Yao, "The terahertz electromagnetically induced transparency-like metamaterials for sensitive biosensors in the detection of cancer cells," Biosens. Bioelectron. **126**, 485–492 (2019).

35. R. P. Pan, C. F. Hsieh, C. L. Pan, and C. Y. Chen, "Temperature-dependent optical constants and birefringence of nematic liquid crystal 5CB in the terahertz frequency range," J. Appl. Phys. **103**, 093523 (2008).

36. Y. K. Srivastava, L. Cong, and R. Singh, "Dual-surface flexible THz Fano metasensor," Appl. Phys. Lett. **111**, 201101 (2017).

37. Y. K. Srivastava, R. T. Ako, M. Gupta, M. Bhaskaran, S. Sriram, and R. Singh, "Terahertz sensing of 7 nm dielectric film with bound states in the continuum metasurfaces," Appl. Phys. Lett. **115**, 151105 (2019).

38. M. Gupta and R. Singh, "Terahertz sensing with optimized Q/V_{eff} metasurface cavities," Adv. Opt. Mater. **8**, 1902025 (2020).

39. D. Dutta, D. De, S. Chaudhuri, and S. K. Bhattacharya, "Hydrogen production by cyanobacteria," Microb. Cell Fact. **4**, 36 (2005).

40. N. Ladygina, E. G. Dedyukhina, and M. B. Vainshtein, "A review on microbial synthesis of hydrocarbons," Process Biochem. **41**, 1001–1014 (2006).

41. B. Gasser and D. Mattanovich, "Antibody production with yeasts and filamentous fungi: on the road to large scale?" Biotechnol. Lett. **29**, 201–212 (2007).

42. S. Y. Chiam, R. Singh, J. Gu, J. Han, W. Zhang, and A. A. Bettiol, "Increased frequency shifts in high aspect ratio terahertz split ring resonators," Appl. Phys. Lett. **94**, 064102 (2009).